Ship and Oil Spill Detection using the Degree of Polarization in Linear and Hybrid/Compact Dual-pol SAR

Reza Shirvany, *Student Member, IEEE,* Marie Chabert, *Member, IEEE*
and Jean-Yves Tourneret, *Senior Member, IEEE*

***Abstract*—Monitoring and detection of ships and oil spills using Synthetic Aperture Radar (SAR) have received a considerable attention over the past few years, notably due to the wide area coverage, and day and night all-weather capabilities of SAR systems. Among different polarimetric SAR modes, dual-pol SAR data are widely used for monitoring large ocean and coastal areas. The degree of polarization (DoP) is a fundamental quantity characterizing a partially polarized electromagnetic field. The performance of the DoP is studied for joint ship and oil spill detection under different polarizations in hybrid/compact and linear dual-pol SAR imagery. Experiments are performed on RADARSAT-2 C-band polarimetric data sets, over San Francisco Bay, and L-band NASA/JPL UAVSAR data, covering the Deepwater Horizon oil spill in the Gulf of Mexico.**

***Index Terms*—Degree of polarization (DoP), depolarization, synthetic aperture radar (SAR), ship detection, oil spill, oil slick, Deepwater Horizon, dual-pol, hybrid, compact polarimetry.**

I. Introduction

Synthetic Aperture Radar (SAR) is a powerful tool strongly employed in a wide variety of applications. There exists a rich literature on maritime surveillance based on SAR polarimetric imagery. Maritime surveillance is of great environmental and economical interest, directly contributing to improve public safety and environmental protection. In particular, efficiently monitoring the ships, oil platforms and oil spills are of critical importance.

Oil spills are highly damaging to the environment and pose serious threats to ecology and wildlife in the marine system. Oil pollution comes partly from frequent illegal ship discharges, and partly from large ship and oil-rig accidents, namely the Prestige tanker disaster (in 2002, northwest coast of Spain), and more recently the British Petroleum (BP) Deepwater Horizon oil spill (in 2010, northern Gulf of Mexico).

Maritime monitoring and surveillance using single- and linear dual-pol SAR modes have been extensively studied using RADARSAT-1, ERS-1/2 and ENVISAT ASAR data, demonstrating very promising results for ship detection and vessel observation. Maritime surveillance in SAR polarimetry can be made more reliable with the advent of new quad-pol (full polarimetric) SAR systems such as the Japanese ALOS-PALSAR, launched in January 2006, the Canadian RADARSAT-2, launched in December 2007, and the German TerraSAR-X, launched in June 2007. Moreover, the future launches of the European Sentinel-1 and the Canadian RADARSAT Constellation Mission (RCM), expected in 2014 with a notable interest in maritime surveillance, will mark a new era for the operational use of SAR data.

Full polarimetric systems alternately transmit two orthogonal polarizations and record both received polarizations, i.e., (HH, HV, VH, VV), where H and V denote the horizontal and vertical polarizations respectively. In conventional dual-pol modes, only two linear polarizations are considered, i.e., (HH, HV), (VH, VV) and (HH, VV). Newly developed dual-pol SAR modes are hybrid and compact dual-pols, promoted in the literature for future SAR missions with the great advantage of providing a wider swath width, and hence greater area coverage compared to quad-pol systems. Souyris et al. [1] introduced the $\pi/4$ compact polarimetric (CP) mode, where the transmitted polarization is the superposition of linear horizontal and vertical polarizations and the received returns are recorded in both horizontal and vertical polarizations (45°H-45°V). In a recent study, Raney [2] suggested a hybrid mode of operation, called CL-pol, with a right (or left) circular polarization on transmission and two linear polarizations on reception (RH, RV). The CL-pol mode is part of the design for the future RADARSAT constellation mission. Different dual-pol modes collect different aspects of the information content of the full polarimetric data, and thus, it is of great importance to study different dual-pol modes and select the appropriate configuration in each particular application.

In each dual-pol mode, the transmitted polarization characterizes the information extracted from a scene. The aim of this paper is to investigate the potential of physically related polarimetric discriminators, the degree of polarization (DoP, $\mathcal{P}$) and the degree of depolarization (DoD, $\overline{\mathcal{P}} = 1 - \mathcal{P}$), for man-made object detection and oil spill observation under different polarizations and incidence angles. The DoP has long been recognized as the most important parameter characterizing a partially polarized electromagnetic field [3, 4]. The DoP can help to determine the nature of the objects that backscatter the electromagnetic field. We demonstrate the potentials of the DoP (equivalently the DoD) to enhance the contrast of man-made objects and oil spills against the surroundings when using different combinations of polarimetric SAR channels. We first analyze and compare the capabilities of DoP for different man-made object detection, i.e., buoys, ships, and

The authors are with the University of Toulouse, IRIT/INP-ENSEEIHT/TéSA, 2 rue Camichel, BP 7122, 31071 Toulouse cedex 7, France (e-mail: reza.shirvany@enseeiht.fr; marie.chabert@enseeiht.fr; jean-yves.tourneret@enseeiht.fr)

oil/gas platforms. Next, we study the oil spill detection and slick type recognition in different dual-pol SAR data. We use L-band data acquired by NASA/JPL Uninhabited Aerial Vehicle Synthetic Aperture Radar (UAVSAR), over northern Gulf of Mexico covering the Deepwater Horizon oil spill, and quad-pol data acquired by RADARSAT-2, over San Francisco Bay. Moreover, we compare the detection results in dual-pol modes with recent results, obtained using quad-pol data, presented by Marino et al. [5, 6].

The paper is organized as follows. In Section II, we review some physical and mathematical definitions, and derive the estimator of the DoP in linear and hybrid/compact dual-pol modes. The data and study areas are presented in Section III. Experimental results and discussions for the detection of buoys, ships, oil-rigs, and oil spills are presented in Section IV. Concluding remarks and future work are addressed in Section V.

II. Theory

The Jones vector [7] for an electromagnetic wave is defined by $\boldsymbol{E} = (E_1, E_2)^T$, where E_1 and E_2 are the orthogonal components of the electric field of the wave. In order to deal with a partially polarized wave the Stokes parameters can be used. In 1852, Stokes [8] introduced four measurable quantities, known as the Stokes parameters, for describing the properties of polarized light. The Stokes parameters in linear polarization basis at the receiver, for a given incident polarization, are given by [9]

$$\begin{aligned} \mathrm{g}_1 &= |E_\mathrm{H}|^2 + |E_\mathrm{V}|^2 \\ \mathrm{g}_2 &= |E_\mathrm{H}|^2 - |E_\mathrm{V}|^2 \\ \mathrm{g}_3 &= 2\Re E_\mathrm{H} E_\mathrm{V}^* \\ \mathrm{g}_4 &= 2\Im E_\mathrm{H} E_\mathrm{V}^* \end{aligned} \tag{1}$$

where E is the complex electric field received in the subscripted polarization, i.e., horizontal or vertical (H or V), * denotes complex conjugate, and $\Re$ and $\Im$ denote the real and imaginary parts of the complex field, respectively. Note that the transmit polarization is not included in the subscripting. The transmit polarization for a traditional dual-pol radar is either H or V, for the CL-pol mode is either left- or right-circular (L and R), and for the $\pi/4$ compact mode is H+V oriented at 45 degrees.

The electric vector $\boldsymbol{E}^\mathrm{r}$ of the received (or backscattered) field and the transmitted (or incident) field $\boldsymbol{E}^\mathrm{t}$ are related by

$$\boldsymbol{E}^\mathrm{r} = \boldsymbol{S}\boldsymbol{E}^\mathrm{t}, \;\; \boldsymbol{S} = \begin{pmatrix} S_\mathrm{HH} & S_\mathrm{HV} \\ S_\mathrm{VH} & S_\mathrm{VV} \end{pmatrix} \tag{2}$$

where $\boldsymbol{S}$ is the scattering matrix, known as the Sinclair matrix [10]. In the bistatic scattering case, the quad-pol scattering vector corresponding to the Sinclair matrix is defined as $\vec{k}_\mathrm{FP} = (S_\mathrm{HH}, S_\mathrm{HV}, S_\mathrm{VH}, S_\mathrm{VV})^T$ [11]. The conventional (linear) dual-pol scattering vectors are obtained straightforwardly from $\vec{k}_\mathrm{FP}$ as

$$\begin{aligned} \vec{k}_\mathrm{DP1} &= (S_\mathrm{HH}, S_\mathrm{HV})^T \\ \vec{k}_\mathrm{DP2} &= (S_\mathrm{VH}, S_\mathrm{VV})^T \\ \vec{k}_\mathrm{DP3} &= (S_\mathrm{HH}, S_\mathrm{VV})^T . \end{aligned} \tag{3}$$

Hybrid/compact dual-pol scattering vectors can be obtained from quad-pol data using (2). In CL-pol mode, for example, a right-circular illumination is achieved by $\boldsymbol{E}^t = 1/\sqrt{2}(1, -j)^T$, and thus $\boldsymbol{E}^r = 1/\sqrt{2}\,(S_\mathrm{HH} - iS_\mathrm{HV}, -iS_\mathrm{VV} + S_\mathrm{VH})^T$. Hence the corresponding scattering vector is achieved by $\vec{k}_\text{CL-pol} = (E_\mathrm{H}, E_\mathrm{V})^T$ where $E_\mathrm{H} = (1, 0)\boldsymbol{E}^r$ and $E_\mathrm{V} = (0, 1)\boldsymbol{E}^r$. The scattering vector for the $\pi/4$ mode can be derived in the same fashion. Hence, hybrid/compact dual-pol scattering vectors are expressed as

$$\begin{aligned} \vec{k}_{\pi/4} &= \frac{1}{\sqrt{2}}\,(S_\mathrm{HH} + S_\mathrm{HV}, S_\mathrm{VV} + S_\mathrm{VH})^T \\ \vec{k}_\text{CL-pol} &= \frac{1}{\sqrt{2}}\,(S_\mathrm{HH} - iS_\mathrm{HV}, -iS_\mathrm{VV} + S_\mathrm{VH})^T . \end{aligned} \tag{4}$$

We note that under the scattering reciprocity, and in the backscatter alignment convention, we have $S_\mathrm{HV} = S_\mathrm{VH}$ [12].

The state of polarization of an electromagnetic wave can be characterized by the DoP expressed, in terms of the Stokes parameters, as

$$\mathcal{P} = \frac{\sqrt{\mathrm{g}_2{}^2 + \mathrm{g}_3{}^2 + \mathrm{g}_4{}^2}}{\mathrm{g}_1}. \tag{5}$$

Mathematically, on the Poincaré sphere, the DoP represents the distance of a normalized Stokes vector's last three components from the origin. The surface of the unit Poincaré sphere corresponds to $\mathcal{P} = 1$, and represents all fully polarized states [13]. Depolarization is associated with a reduction in the DoP of incident states. The DoD is defined as $\overline{\mathcal{P}} = 1 - \mathcal{P}$. A depolarizing interaction causes fully polarized Stokes states on the surface of the Poincaré sphere to emerge with $\mathcal{P} < 1$, and thus $\overline{\mathcal{P}} > 0$. In brief, the wave is totally depolarized for $\overline{\mathcal{P}} = 1$ ($\mathcal{P} = 0$), totally polarized for $\overline{\mathcal{P}} = 0$ ($\mathcal{P} = 1$), and partially polarized when $\overline{\mathcal{P}}, \mathcal{P} \in]0, 1[$. The DoP, and thus the DoD, are invariant with respect to the choice of orthogonal polarization basis at the receiver. However, DoD and DoP are dependent of the transmit polarization. Hence, the nature of the application and targets of interest determine the optimal transmit polarization.

The DoP and DoD are estimated in each dual-pol mode by

$$\begin{aligned} \mathcal{P} &= \frac{\sqrt{\widehat{\alpha}_2^2 + \widehat{\alpha}_3^2 + \widehat{\alpha}_4^2}}{\widehat{\alpha}_1} \\ \overline{\mathcal{P}} &= 1 - \mathcal{P} \end{aligned} \tag{6}$$

with $\widehat{\alpha}_l = \frac{1}{n}\sum_{j=1}^{n} \mathrm{g}_l\,[j]$, $l = 1, \ldots, 4$, where n is the number of samples used for the estimation, and $\mathrm{g}_l\,[j]$ is the l-th Stokes parameter associated with the j-th pixel. In other words, $\widehat{\alpha}_l$ is calculated for each pixel by using a sliding square window centered on the considered pixel, and computing the empirical mean over the n pixels contained in the window. In the next section, the detection performance of DoP maps in different hybrid/compact and linear dual-pol modes are studied for different scenarios.

III. Data and Study Sites

In this study, the sensitivity of the DoP with respect to different polarizations is investigated for the discrimination

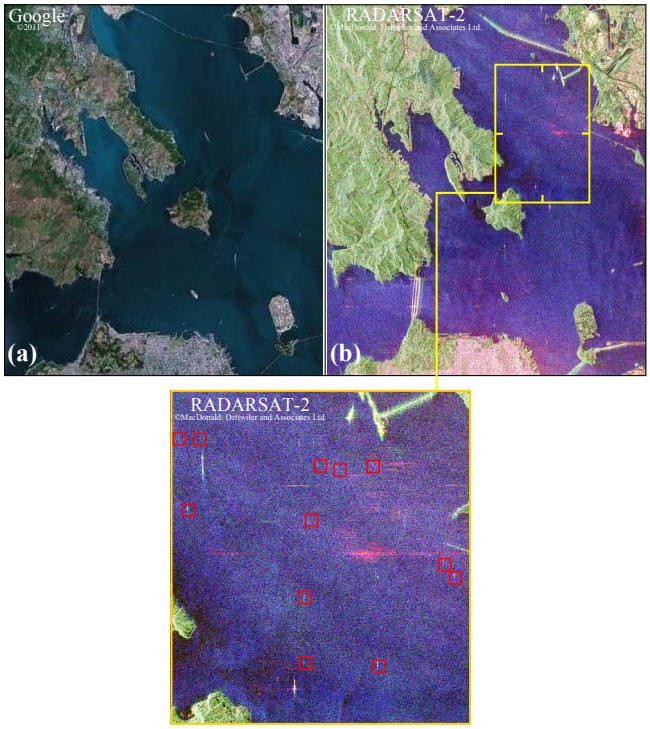

Fig. 1. [Color online] San Francisco Bay, CA. USA. (a) Google Earth™ image of the area. (b) Pauli RGB image of the RADARSAT-2 fully polarimetric data set (Red, $|S_{HH} - S_{VV}|$; Green, $|S_{HV} + S_{VH}|$; Blue, $|S_{HH} + S_{VV}|$). Red boxes outline 12 buoys of interest. The original image has a size of 1816×3600 pixels.

of man-made objects and oil spills from the sea surface. We estimate the DoP in hybrid/compact and linear dual-pol SAR modes and compare the detection performance of these modes for different scenarios. We use C-band data acquired by RADARSAT-2, as well as L-band data acquired by NASA/JPL UAVSAR. RADARSAT-2 is a Canadian C-band SAR satellite launched in December, 2007. It provides many operating modes, including linear dual- and quad-pol modes, and supports right- and left-look imaging. The NASA/JPL UAVSAR, operational since 2007, is a reconfigurable fully polarimetric L-band (1.26 GHz, 24 cm wavelength) airborne system with a range bandwidth of 80 MHz (2 m range resolution), and a range swath greater than 16 km.

The RADARSAT-2 data set is acquired in fine quad-pol mode over San Francisco Bay, California (+37°45'0"N, +122°17'0"W). The Google Earth and Pauli RGB images of this data set are shown in Fig. 1. RADARSAT-2 data are used for detection of ships, boats and buoys. Furthermore, oil/gas platform detection is studied using NASA/JPL UAVSAR data sets over northern Gulf of Mexico, Mississippi River Delta, Louisiana (+29°0'43.56"N, +89°15'33.12"W). The Google Earth and Pauli RGB images of this data set are shown in Fig. 6. We analyze the depolarization signatures of oil spills, under different incidence angles and polarizations, using the Deepwater Horizon oil spill data (+28°44'11.86"N, +88°21'57.59"W), acquired by NASA/JPL UAVSAR on June 22-23, 2010. The Deepwater Horizon oil spill, occurred on April 20, 2010 in the Gulf of Mexico, is by far the worst oil spill in U.S. history, with over 200 million gallons of leaked oil along the coastal areas of Louisiana, Mississippi, Alabama, and Florida. The Pauli RGB image of the oil spill study region is shown in Fig. 8. All original NASA/JPL UAVSAR data sets are acquired in quad-pol mode.

IV. Experimental Results and Discussion

A. Buoy Detection

Buoys are distinctively shaped floating devices with many different purposes. In this section, we consider the buoy detection task, since there exist accurate nautical charts reporting the exact position of the buoys via different systems. In particular, we use nautical charts from National Oceanic and Atmospheric Administration (NOAA) as ground truths. Fig. 2(a) shows a NOAA nautical chart over a test region in San Francisco Bay with 12 buoys of interest (red boxes). The maps of the DoP obtained over this region, for linear and hybrid/compact dual-pol modes, are shown in Figs. 2(b)–(f). Thresholds were manually chosen so that a maximum number of targets may be visible. These results suggest that hybrid/compact dual-pol modes are more performant than traditional linear dual-pol modes; most of the buoys which can hardly be seen in linear dual-pol modes, are easily distinguished in hybrid/compact modes.

The latter is further demonstrated in Figs. 3 and 4. These figures respectively show the DoD surfaces for Southampton Shoal day mark (height = 32 ft/9.75m, marked as T1 in Fig. 2(a)), and Southampton Shoal Channel Entrance buoy (T2). We clearly see the gain of performance for buoy detection when using hybrid/compact dual-pol data compared to linear (HH, HV) and (VH, VV) data. We note that the results from (HH, VV) mode are closely comparable to hybrid/compact modes.

B. Ship Detection

In this section we study the performance of the DoP maps in a ship detection context. For this purpose, we compare the DoP maps of San Francisco Bay region to the results recently reported by Marino et al. [5, 6]. Fig. 5(a) shows the Pauli RGB images of a region of interest from RADARSAT-2 San Francisco Bay data set. Figs. 5(b)–(f) show the maps of the DoP obtained in hybrid/compact and linear dual-pol modes over the test region (thresholds were manually chosen so that a maximum number of targets may be visible). Fig. 5(g) shows the ship detection results reported by Marino et al. [5, 6] obtained using a notch filter based on quad-pol SAR data. In these figures, boxes indicate potential ships; solid (white) boxes indicate targets that are visible in all modes whereas dashed (black) boxes indicate less- or non-visible targets in linear dual-pol modes. We see that most of the ships detected using the quad-pol method (Fig. 5(g)) are not visible in the (HH-HV) and (VH-VV) dual-pol modes (black, dashed boxes) whereas they are clearly seen in (HH-VV) and hybrid/compact dual-pol modes. We also note that the ship detection results based on the estimation of the DoP in hybrid/compact dual-pol modes are closely comparable to the results obtained using quad-pol data (which benefit from the full polarimetric

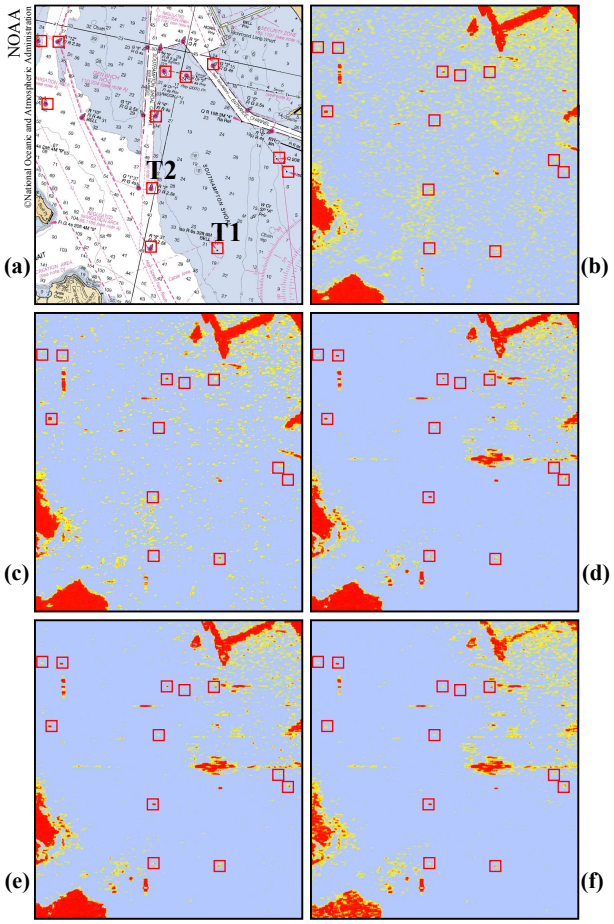

Fig. 2. [Color online] (a) NOAA nautical chart showing the position of the buoys. (b–f) Maps of the degree of polarization over the San Francisco Bay test area, outlined in Fig. 1(b), in different hybrid/compact and linear dual-pol modes; (b) HH-HV (c) VH-VV (d) HH-VV (e) CL-pol. (f) $\pi/4$.

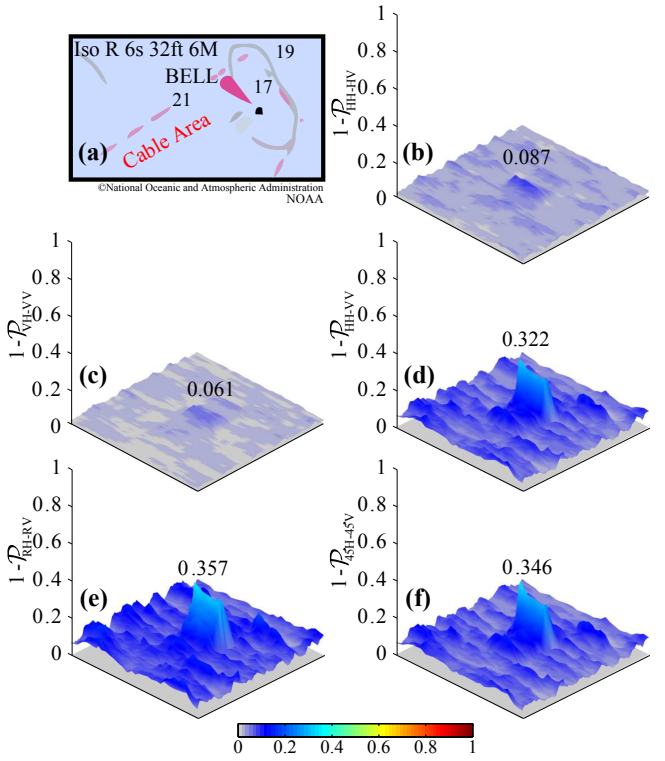

Fig. 3. [Color online] San Francisco Bay, CA. USA. (a) NOAA nautical chart showing the position of Southampton Shoal day mark (T1). (b)–(f) The degree of depolarization in different hybrid/compact and linear dual-pol modes; (b) HH-HV (c) VH-VV (d) HH-VV (e) CL-pol (f) $\pi/4$

information of the scene). These results are in agreement with the results obtained in the buoy detection case. However, we emphasis that the ship detection problem is slightly different from the previous buoy detection context; in particular, ships are much bigger than buoys, and thus, they can introduce a preferred direction. Therefore, some ships, because of there alignment, may be more visible in some dual-pol modes than the others. This issue is to be addressed in future work by studying different ship detection scenarios in the presence of ground truth.

C. Oil-rig Detection

Efficiently identifying the existence and position of oil and gas platforms after tropical events is of critical importance. In the context of oil-rig detection, Gulf of Mexico with nearly 4000 active oil and gas platforms is an interesting study case. Fig. 6 shows the Google Earth™ and Pauli RGB images of a test region in northern Gulf of Mexico, along with a NOAA nautical chart reporting the position of oil and gas platforms. Most of the targets are bright enough to be visible on the Pauli RGB image. The DoD surfaces showing two oil platforms (marked as T3 in Fig. 6) are shown in Fig. 7. Once again, we notice that hybrid/compact and (HH, VV) modes clearly detect the oil-rigs whereas (HH, HV) and (VH, VV) modes are less performant. We note that DoP signatures are representative of different scattering mechanisms in a scene. Hence, the DoP surfaces can also help in target identification (for example distinguishing between buoys, ships, and oil-rigs). This is an interesting subject for future work.

D. Oil Spill Detection and Identification

Oil does not mix with water, and initially spreads as thin layers on the surface of the ocean. In this section we study the depolarization signatures of oil spills and clear water under different incidence angles and transmit polarizations. We use homogeneous regions of oil and water, covering all the incidence angle range, i.e., from 25 to 65 degrees (near- to far-range), as shown in Fig. 8. The depolarization profile of these regions are shown in Fig. 9. All dual-pol modes discriminate water and oil for most of the incidence angle range. These results suggest that HH-VV mode outperforms other modes in distinguishing oil and water for shallow incidence angles whereas in steeper incident angles HH-HV outperforms other modes. The detection results from hybrid/compact dual-pol modes (CL-pol and $\pi/4$) are close to HH-VV. We notice that the clear water depolarizes the incident wave more than oil for steep incidence angles, and less than oil for shallow incidence angles. The transition incidence angle is around 40 degrees.

Identifying the color, structure, and consistency of oil on water can help to determine the oil type, the amount of time

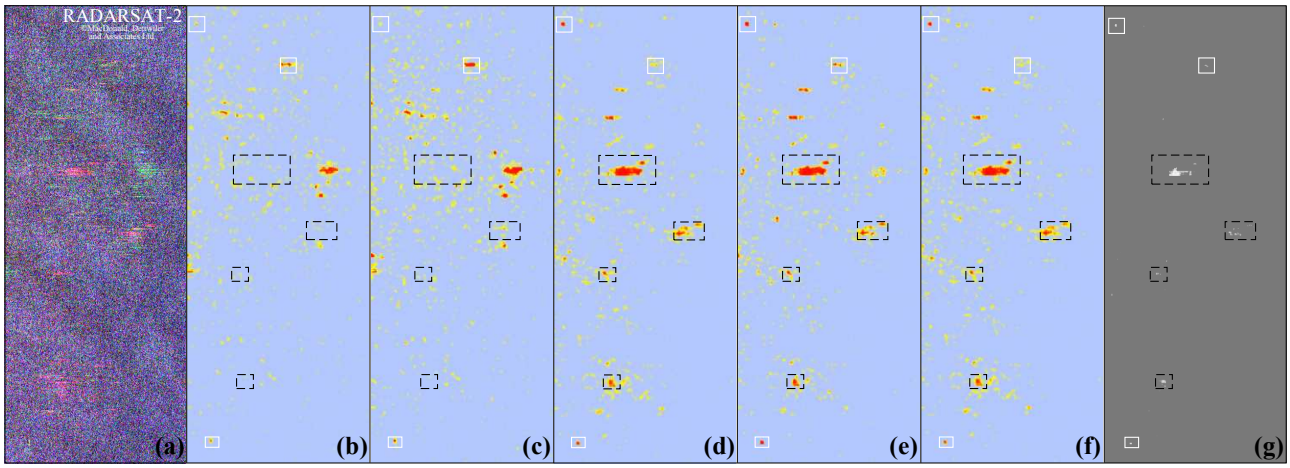

Fig. 5. [Color online] (a) Pauli RGB image of a test area from San Francisco Bay, RADARSAT-2 fully polarimetric data set. (b)–(f) Maps of the degree of polarization over the test area in different hybrid/compact and linear dual-pol modes; (b) HH-HV. (c) VH-VV. (d) HH-VV. (e) CL-pol. (f) $\pi/4$. (g) Ship detection results, based on quad-pol data, reported by Marino et al. [5, 6]. Boxes indicate potential ships; solid (white) boxes indicate targets that are visible in all modes whereas dashed (black) boxes indicate less- or non-visible targets in linear dual-pol modes.

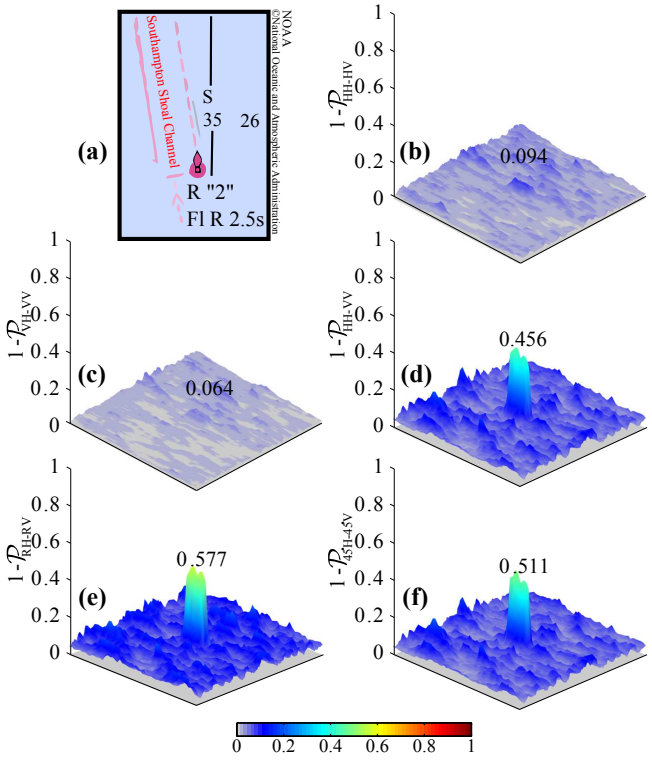

Fig. 4. [Color online] San Francisco Bay, CA. USA. (a) NOAA nautical chart showing the position of Southampton Shoal Channel Entrance buoy (T2). (b)–(f) The degree of depolarization in different hybrid/compact and linear dual-pol modes; (b) HH-HV (c) VH-VV (d) HH-VV (e) CL-pol (f) $\pi/4$

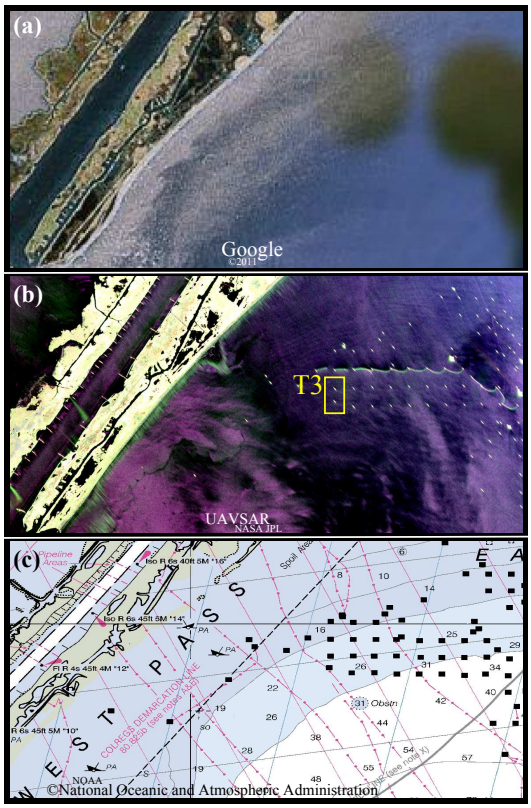

Fig. 6. [Color online] Mississippi River Delta, Louisiana, USA. (a) Google Earth™ image of the area. (b) Pauli RGB image of the NASA/JPL UAVSAR fully polarimetric data set (Red, $|S_{HH} - S_{VV}|$; Green, $|S_{HV} + S_{VH}|$; Blue, $|S_{HH} + S_{VV}|$). (c) NOAA nautical chart showing the position of the oil platforms. The original image has a size of 1600 × 800 pixels.

it has been on the water, and other information, critical to improve the oil recovery process. The thinnest possible oil layer is called sheen which dampens out the surface waves and gives the water a reflective appearance. Thicker oil layers are called rainbow, metallic, transitional, and dark oil slick. Depolarization maps of oil spills are further studied in Fig. 10 for oil property recognition in different dual-pol SAR modes.

In each figure, three regions of interest (R1, R2 and R3) are outlined. All depolarization maps reveal the oil structures and properties in different dual-pol modes with HH-VV giving the maximum depolarization contrast between dark oil and clear water. Using these depolarization maps, we can clearly

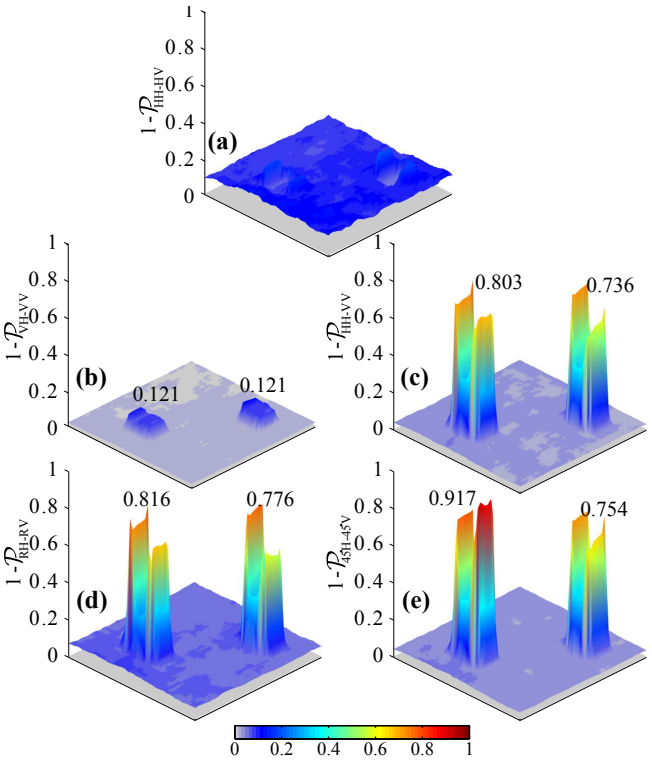

Fig. 7. [Color online] The degree of depolarization for oil platforms (T3) in the Mississippi River Delta, Louisiana, USA. (a) HH-HV (b) VH-VV (c) HH-VV (d) CL-pol (e) $\pi/4$

recognize the oil sheens along the edges (in R1 regions), the narrow bands of oil (in R2 regions) revealing the wind direction, and also dark oil patches (in R3 regions).

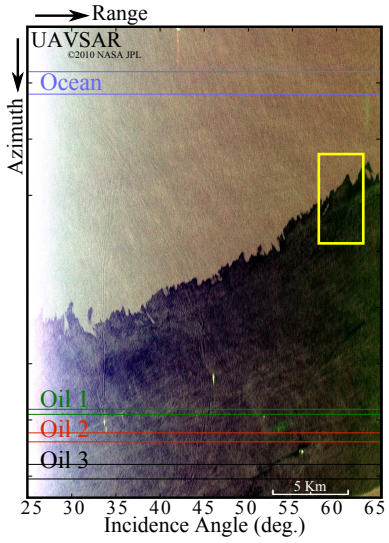

Fig. 8. [Color online] Pauli RGB image of the NASA/JPL UAVSAR fully polarimetric data set from the Deepwater Horizon oil spill in northern Gulf of Mexico, USA. (Red, $|S_{HH} - S_{VV}|$; Green, $|S_{HV} + S_{VH}|$; Blue, $|S_{HH} + S_{VV}|$). The region in the yellow box is further studied in Fig. 10. The original image has a size of 3151×4201 pixels.

The proposed polarimetric framework is of great interest for maritime surveillance and monitoring using dual-pol SAR

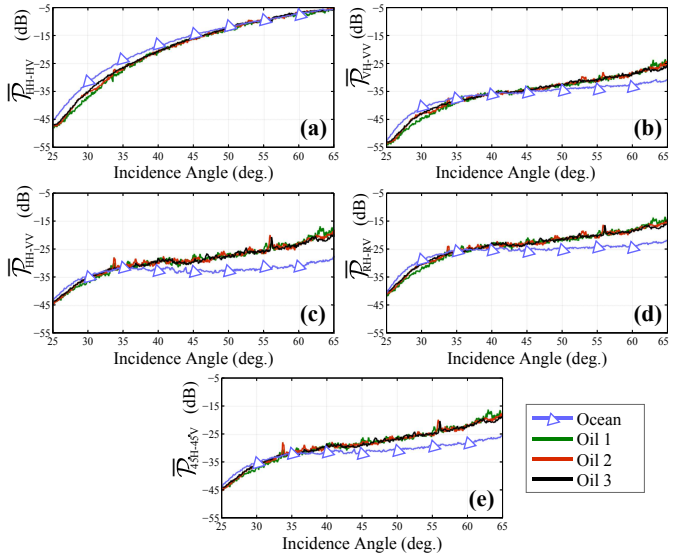

Fig. 9. [Color online] Depolarization $\overline{\mathcal{P}}$ (dB) versus incidence angle (deg.) for ocean and oil regions in different hybrid/compact and linear dual-pol modes. (a) HH-HV. (b) VH-VV. (c) HH-VV. (d) RH-RV. (e) 45°H-45°V. Regions are shown in Fig. 8.

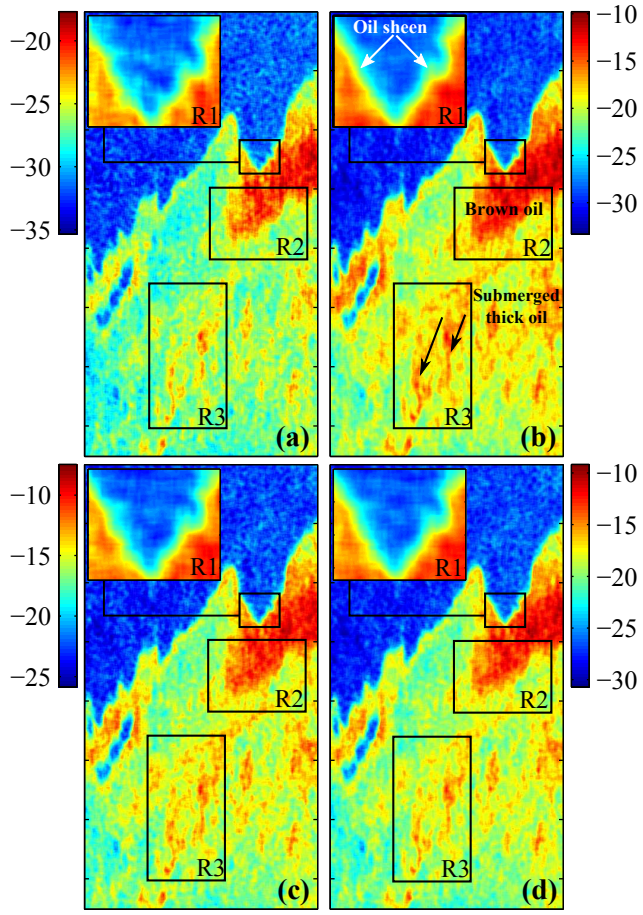

Fig. 10. [Color online] Oil slick property/type recognition using the degree of depolarization $\overline{\mathcal{P}}$ (dB) in dual-pol SAR. (a) VH-VV. (b) HH-VV. (c) RH-RV. (d) 45°H-45°V. The region is an excerpt of UAVSAR data set (outlined in Fig. 8). A sliding window covering $n = 7 \times 7$ pixels is used.

data. In particular, the joint detection of ships and oil spills in large coastal and ocean areas. Future work will concentrate on analyzing the potential of DoP for man-made object detection, under different incidence angles, in multifrequency L-, C-, and X-band polarimetric SAR.

V. Conclusion

The degree of polarization was used to detect the features, such as man-made objects and oil spills, with different polarimetric signatures compared to the sea clutter. The detection performance of the degree of polarization was studied in different hybrid/compact and linear dual-pol SAR modes. Experiments were performed on RADARSAT-2 C-band polarimetric data sets, over San Francisco Bay, and L-band NASA/JPL UAVSAR data, covering the Deepwater Horizon oil spill in the Gulf of Mexico. Experimental results suggest that hybrid/compact and (HH, VV) dual-pol modes deliver better detection performance compared to conventional dual-pol modes, i.e., (HH, HV) and (VH,VV). Investigated polarization signatures are of great interest in joint detection of ships and oil spills, using dual-pol SAR data, in large coastal and ocean areas under all-weather conditions. Future work will concentrate on analyzing and comparison of polarization signatures of ships and oil spills in multifrequency L-, C-, and X-band polarimetric SAR data, and discrimination between oil spills and look-alikes.

Acknowledgment

We would like to thank Ridha Touzi and Armando Marino for the interesting discussions. We also acknowledge NASA Jet Propulsion Laboratory (JPL) and Alaska Satellite Facility (ASF) for providing UAVSAR data, and MacDonald, Dettwiler and Associates Ltd. (MDA), for making available the RADARSAT-2 data used in this paper.

References

[1] J.-C. Souyris, P. Imbo, R. Fjortoft, S. Mingot, and J.-S. Lee, "Compact polarimetry based on symmetry properties of geophysical media: the $\pi/4$ mode," *IEEE Trans. Geosci. Remote Sens.*, vol. 43, no. 3, pp. 634–646, Mar. 2005.

[2] R. Raney, "Hybrid-polarity SAR architecture," *IEEE Trans. Geosci. Remote Sens.*, vol. 45, no. 11, Nov. 2007.

[3] R. C. Jones, "A new calculus for the treatment of optical systems: a more general formulation and description of another calculus," *J. Opt. Soc. Am.*, vol. 37, no. 2, pp. 107–110, 1947.

[4] E. Wolf, "Coherence properties of partially polarized electromagnetic radiation," *Nuovo Cim.*, vol. 13, no. 6, pp. 1165–1181, Sep. 1959.

[5] A. Marino, N. Walker, and I. Woodhouse, "Ship detection using SAR polarimetry. the development of a new algorithm designed to exploit new satellite SAR capabilities for maritime surveillance." in *Proc. of SeaSAR'10*, Rome, Italy, Jan. 2010.

[6] ——, "Ship detection with RADARSAT-2 quad-pol SAR data using a notch filter based on perturbation analysis," in *Proc. of IGARSS'10*, Hawaii, USA, Jul. 2010.

[7] R. C. Jones, "A new calculus for the treatment of optical systems," *J. Opt. Soc. Am.*, vol. 31, no. 7, pp. 488–493, Jul. 1941.

[8] G. G. Stokes, "On the composition and resolution of streams of polarized light from different sources," *Trans. Camb. Philosoph. Soc.*, vol. 9, pp. 399–416, 1852.

[9] P. E. Green Jr, "Radar measurements of target scattering properties," in *Radar astronomy*, J. V. Evans and T. Hagfors, Eds. New York: McGraw-Hill, 1968, pp. 1–78.

[10] A. Guissard, "Mueller and Kennaugh matrices in radar polarimetry," *IEEE Trans. Geosci. Remote Sens.*, vol. 32, no. 3, pp. 590–597, May 1994.

[11] J.-S. Lee and E. Pottier, *Polarimetric Radar Imaging: From Basics to Applications*. CRC Press, 2009.

[12] S. V. Nghiem, S. H. Yueh, R. Kwok, and F. K. Li, "Symmetry properties in polarimetric remote sensing," *Radio Science*, vol. 27, pp. 693–711, Oct. 1992.

[13] C. Brosseau, *Fundamentals of Polarized Light: A Statistical Optics Approach*. John Wiley and Sons, 1998.